Connecting the terrestrial gamma-ray flash source strength and observed fluence distributions

B. E. Carlson,[1] T. Gjesteland,[1] and N. Østgaard[1]

Received 7 September 2011; revised 26 October 2011; accepted 15 November 2011; published 21 January 2012.

[1] Terrestrial gamma-ray flashes (TGFs) as observed by satellites have a broad fluence distribution. This fluence distribution is not trivially related to the source strength distribution, since even a very strong TGF may still be observed at low fluence if the source is far from the satellite. In this paper we connect the source strength distribution with the observed fluence distribution by calculating the effective size and probability of detection of TGFs as a function of their source strength. For sources at a single altitude, power law distributions of source strength give softer power law distributions in observed fluence with especially pronounced softening for very hard source power law indices. This result holds even with broad source altitude distributions in regions of the fluence distribution away from the peak fluence since such regions tend to be dominated by TGFs produced in a relatively narrow range of higher altitudes.

Citation: Carlson, B. E., T. Gjesteland, and N. Østgaard (2012), Connecting the terrestrial gamma-ray flash source strength and observed fluence distributions, *J. Geophys. Res.*, *117*, A01314, doi:10.1029/2011JA017122.

1. Introduction

[2] Terrestrial gamma-ray flashes (TGFs) are intense sub-millisecond pulses of photons with a very hard photon energy spectrum as observed by satellites [*Fishman et al.*, 1994; *Smith et al.*, 2005; *Marisaldi et al.*, 2010; *Briggs et al.*, 2010]. The hard average spectrum can be well-explained as bremsstrahlung from populations of energetic electrons at 15–20 km altitude [*Dwyer and Smith*, 2005; *Carlson et al.*, 2007; *Østgaard et al.*, 2008; *Gjesteland et al.*, 2010]. These electrons are likely accelerated by strong electric fields in thunderclouds as lightning-associated electrical activity typically occurs within 1 ms and 300 km of TGF observation [*Inan et al.*, 1996; *Cummer et al.*, 2005; *Cohen et al.*, 2006; *Inan et al.*, 2006; *Stanley et al.*, 2006; *Cohen et al.*, 2010; *Connaughton et al.*, 2010]. The exact production mechanism is not understood, though the strong electric fields close to the lightning channel may play a role [*Moss et al.*, 2006; *Dwyer*, 2008; *Carlson et al.*, 2009, 2010; *Chanrion and Neubert*, 2010; *Celestin and Pasko*, 2011],as may the large electric potential differences that exist in thunderclouds [*Dwyer*, 2007, 2008]. Recent observations of lightning electrical activity closely associated with TGFs suggest TGF production during the initial stage of positive intracloud lightning (i.e. moving negative charge upward) [*Shao et al.*, 2010; *Lu et al.*, 2010, 2011; *Cummer et al.*, 2011], at least for some TGFs.

[3] In the context of the unknown production mechanism, constraints on the TGF source are particularly valuable. One important unknown is the distribution of intrinsic TGF source strengths. This distribution must in some way be related to the physics of the source, so any constraints on the source strength distribution are very useful. Unfortunately, the distribution of observed TGF fluence (photons per area) is not directly related to the source strength, since the location and directionality of the source are unknown. A very strong TGF may still be observed to have low fluence if the source is especially far from the satellite or is especially deep in the atmosphere while a low-strength TGF may be observed to have especially high fluence if the source is at high altitude and is directly beneath the satellite. An analysis of the source strength distribution must therefore account for the likelihood of TGF observation with various geometries. In this paper we study this likelihood and use it to determine the distribution of observed TGF fluences given a variety of source strength and altitude distributions. We do this first for sources at a single altitude by simulating the size of the region over which a TGF would be detectable, calculating the probability of TGF detection as a function of this effective size of the TGF, and combining the results with simple probability theory to determine the relevant distributions. The results of source altitude distributions are then constructed by superposition of results at single altitudes. Throughout this work "fluence" refers to the intensity of an observation (particles per area) and "strength" refers to the total energy released as gamma-rays by the source, while "hard" and "soft" refer respectively to distributions that emphasize high and low fluence or strength.

2. Effective TGF Size

[4] The size of a TGF at satellite orbit is effectively the area over which the fluence of TGF photons exceeds some minimum detectable fluence. The TGF fluence at satellite

[1]Department of Physics and Technology, University of Bergen, Bergen, Norway.

0148-0227/12/2011JA017122

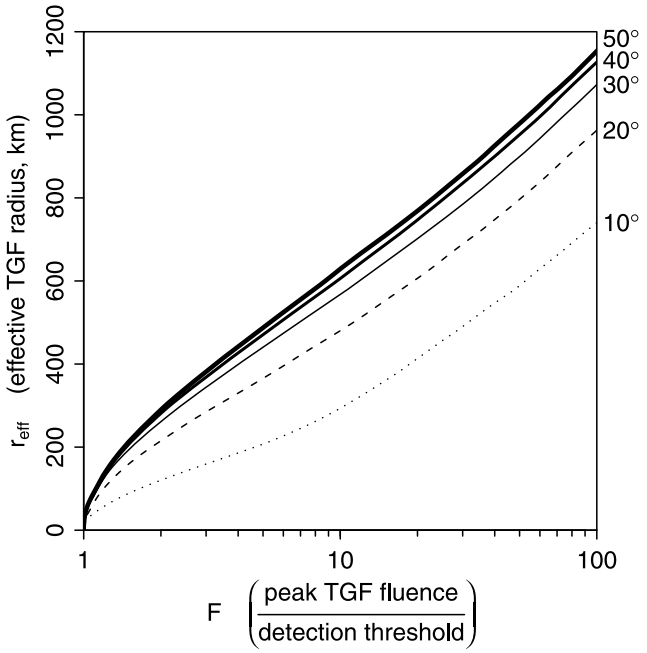

Figure 1. Effective size of a TGF (measured by r_{eff}, the effective radius at satellite altitude) vs the source strength (measured by F, the peak fluence divided by the minimum detectable fluence). The dotted, dashed, solid thin, and solid medium, and solid thick curves correspond to sources with σ_θ = 10°, 20°, 30°, 40°, and 50° respectively as marked at right. The results shown are for sources at 20 km altitude.

altitude can be determined by Monte Carlo simulation of TGF photon escape from the atmosphere, here carried out with GEANT4 [*Agostinelli et al.*, 2003]. As the exact parameters of the initial population of TGF photons are unknown, we assume a point source of photons with an energy distribution derived by bremsstrahlung from relativistic runaway electron avalanche simulations and consistent with satellite observations of TGFs [*Carlson et al.*, 2007]. Such a bremsstrahlung source is consistent with average TGF observations only if the source falls at 15–20 km altitudes, so for the moment we neglect the spread in source altitude and place our point source at 20 km altitude (altitude distributions are treated in section 5). The initial photons are assumed to be beamed upward with solid angle distribution $dN/d\Omega \propto \exp(-\theta^2/2\sigma_\theta^2)$ where θ is the zenith angle and σ_θ measures the width of the beam. σ_θ is chosen to range from 10° to 50°, including relatively broad beams most consistent with satellite observations [*Carlson et al.*, 2007; *Hazelton et al.*, 2009; *Gjesteland et al.*, 2011]. The simulations are carried out in an MSIS atmosphere [*Hedin*, 1991] around a spherical earth. The photons that reach satellite altitude (here taken to be 550 km) are recorded and used to determine the fluence distribution at satellite altitude by histogram or kernel density estimation.

[5] The size of the area over which this fluence exceeds the minimum detectability threshold depends both on the satellite sensitivity and on the intrinsic strength of the TGF. However, since for the present we assume a single source altitude, the intrinsic strength of the TGF is directly proportional to the peak fluence of the TGF (i.e. observation directly above the source). As such, we can measure the inherent TGF strength as the peak fluence which we normalize over the detection threshold. Given a hypothetical TGF with source strength such that its peak fluence is 20× the minimum detectability threshold, we can determine the effective size of the TGF as the size of the region within which the fluence is above 1/20 = 5% of the peak fluence, for instance by reading a contour plot. This size, r_{eff}, is shown vs intensity of the TGF for several different σ_θ in Figure 1.

3. Probability of TGF Detection

[6] The likelihood of detection of a given TGF is most directly measured by the probability of finding a satellite within the area illuminated by the TGF. This probability depends on the location of the TGF and the satellite orbit inclination and can easily be assessed by Monte Carlo averaging by counting the fraction of randomly drawn satellite positions that fall within the TGF area. Here we take the TGF area to be a circle at satellite orbit with a given radius and draw satellite positions by selecting a random orbital phase, calculating the resulting satellite position, and placing Earth beneath the satellite with a random longitude. We use an orbital inclination of 26° as from the Fermi Gamma-ray Space Telescope. We also remove any satellite positions that happen to be located in the South Atlantic Anomaly as TGFs cannot be detected when the background radiation is so intense [e.g., see *Briggs et al.*, 2010, Figure 1]. This probability measurement must be repeated for a variety of TGFs drawn from the overall distribution of TGFs. Here we approximate such a sampling by using the spacecraft locations for the 820 TGFs seen by the Reuven Ramaty High Energy Solar Spectroscopic Image (RHESSI) given by *Grefenstette et al.*[2009]. Though this sampling is not unbiased, being affected for example by the coverage of the RHESSI satellite and decimation of the RHESSI data stream at high latitudes, these bias effects are limited over the ±26° latitude region outside the South Atlantic Anomaly covered by our fictional satellite. A map of these TGFs colored by our measured probability of detection is shown in Figure 2, assuming for example that the effective radius of a TGF is 300 km.

[7] This probability of detection measurement can be used to calculate the mean probability of detection and can be repeated for a variety of effective TGF sizes. The mean probability of detection can then be expressed as a function of the effective TGF size, $P_{\text{d}}(r_{\text{eff}})$. This function, together with the effective size as a function of strength ($r_{\text{eff}}(F)$ as in Figure 1) can be used to give the probability of detection as a function of strength: $P_{\text{d}}(F) = P_{\text{d}}(r_{\text{eff}}(F))$. This probability of detection function contains all the information necessary to construct the connection between the distributions of source strength and observed fluence.

4. Distributions of Source Strength and Observed Fluence

[8] The distribution of observed fluence can be calculated given a distribution of source strength as

$$\frac{dN_{\text{d}}}{dF_{\text{d}}} = \int_{F_{\min}}^{F_{\max}} dF \frac{dN(F)}{dF} \frac{dP_{\text{d}}(F_{\text{d}}|F)}{dF_{\text{d}}}, \tag{1}$$

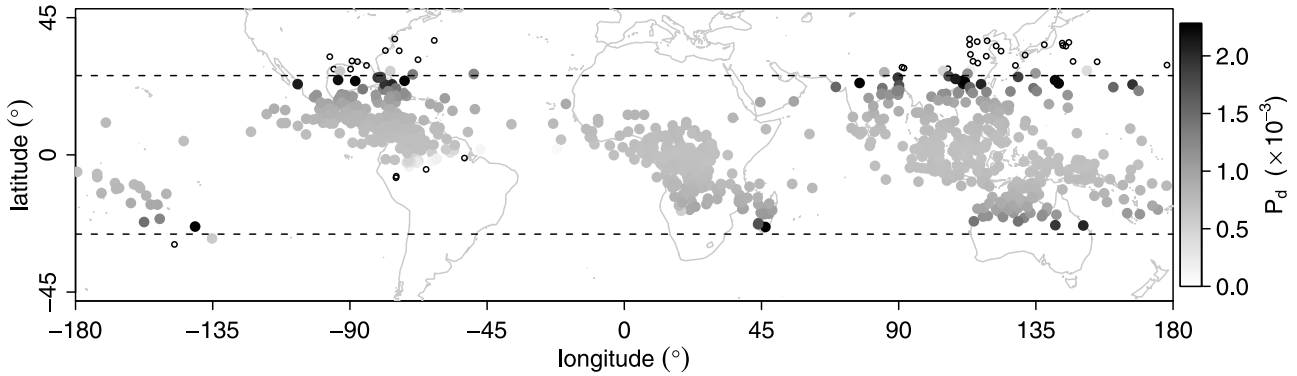

Figure 2. Map of RHESSI TGFs colored by probability of detection as measured for 300 km effective TGF radius. The open circles denote RHESSI TGFs not detectable by our hypothetical satellite with its 26° orbit inclination (shown as dotted lines). The mean probability of detection for this set of TGFs is $P_d(r_{eff} = 300\ km) \sim 8 \times 10^{-4}$.

where dN_d/dF_d is the observed fluence distribution, dN/dF is the source strength distribution, and $dP_d(F_d|F)/dF_d$ is the probability density of observing a TGF to have fluence F_d given that the TGF source strength (i.e. peak fluence) is F.

[9] The conditional probability $dP_d(F_d|F)/dF_d$ can be constructed from $P_d(F)$. First, note that the probability for observation of a TGF of strength F at fluence at least F_d is $P_d(F/F_d)$. The change in probability of detection due to an infinitesimal change in F_d therefore gives

$$\frac{dP_d}{dF_d} = \frac{P_d\left(\frac{F}{F_d}\right) - P_d\left(\frac{F}{F_d+dF_d}\right)}{dF_d}. \quad (2)$$

Defining $x = F/F_d$ and expressing $P_d(\frac{F}{F_d+dF_d})$ as $P_d(x) + \frac{dP_d}{dx}\frac{dx}{dF_d}dF_d$ and noting that $\frac{dx}{dF_d} = -\frac{F}{F_d^2}$ gives

$$\frac{dP_d(F_d|F)}{dF_d} = \frac{dP_d(x)}{dx}|_{F/F_d}\frac{F}{F_d^2}. \quad (3)$$

The derivative $dP_d(x)/dx$ can be evaluated numerically from the results shown above. Since TGFs with $F < 1$ are not detectable and fluences higher than 100× the detection threshold have not been observed, we use $F_{min} = 1, F_{max} = 100$. The only remaining unknown term in equation (1) is dN/dF, the source strength distribution.

[10] There are several obvious test distributions for dN/dF to use to study the resulting observed fluence distributions (dN_d/dF_d) of TGFs. First, consider delta functions in source strength, i.e. populations of TGF sources with a single strength. The observed fluence distributions resulting from three different source strengths are shown in Figure 3. The observed fluence distribution for broader beamed sources is close to a power law $dN_d/dF_d \propto F_d^{-\alpha_d}$ with index $\alpha_d \sim 1.5$, though the $\sigma_\theta = 10°$ (dotted) case gives more of a broken power law with the behavior of near-peak-fluence measurements dominated by the narrow peak of unscattered photons and the lower-fluence measurements largely determined by the broad spread of scattered TGF photons.

[11] The next logical source strength distribution is a power law, $dN/dF \ F^{-\alpha}$, as shown for example for $\sigma_\theta = 30°$ in Figure 4. Regions of the plot away from $F_{max} = 100$ have approximately constant slope, meaning the observed fluence distributions are also power laws with index α_d defined similar to α. The power law index of the distributions of observed fluence is shown vs the corresponding power law index of source strength in Figure 5. For soft distributions of source strength, the power law indices α and αd are approximately equal, but the observed fluence distribution is significantly softer when $\alpha \lesssim 2.5$. For extremely hard distributions of source strength, the observed fluence power law index approaches a minimum value approximately equal to the power law index seen in the delta-function response.

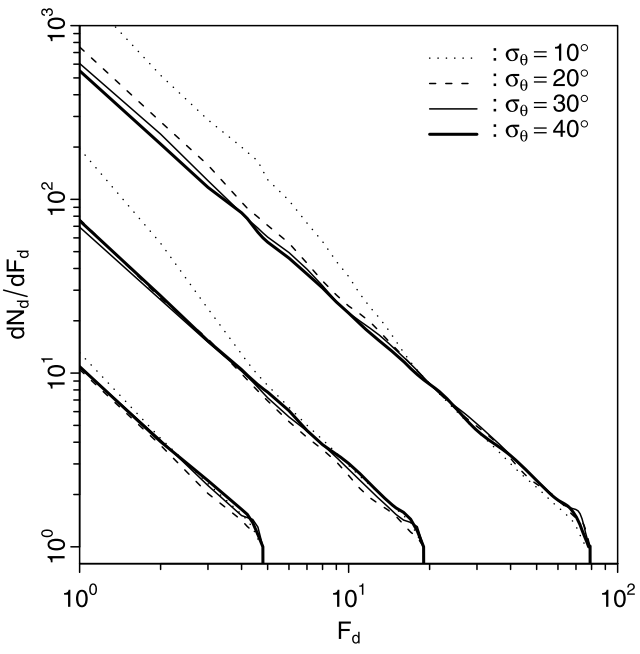

Figure 3. The observed fluence distribution dN_d/dF_d resulting from TGF source populations at 20 km altitude with identical strength, i.e. delta function distributions of source strength at F = 5, 20, and 80. The dotted, dashed, solid thin, and solid thick curves correspond to the expected observations of sources with σ_θ = 10°, 20°, 30°, and 40° respectively, while the 40° and 50° cases overlap. The dN_d/dF_d curves for broader beams are approximately power laws with index $\alpha_d \sim 1.5$.

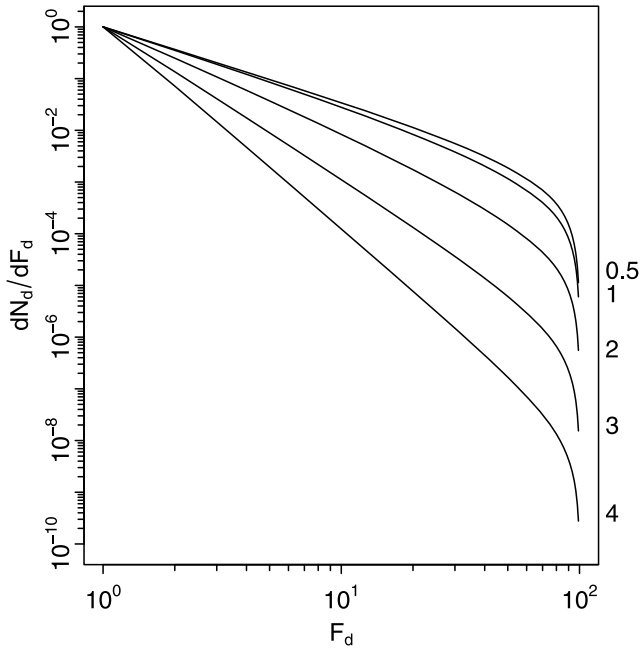

Figure 4. Sample observed fluence distribution dN_d/dF_d resulting from sources at 20 km altitude with power law distributions of source strength $dN/dF \propto F^{-\alpha}$ with, from bottom to top, α = 4, 3, 2, 1, and 0.5 as marked at right. Here the source is taken to have $\sigma_\theta = 30°$. The cut off at F_d = 100 is due to the use of F_{max} = 100 in equation (1).

This implies that for very hard source strength distributions, observations are dominated by the strongest sources and the resulting fluence distribution approaches that of sources at a single high strength.

5. Altitude Distribution Effects

[12] Up to this point we have assumed that every TGF was produced at 20 km altitude. In reality there will be some distribution in production altitudes, with lower altitudes requiring a higher strength to achieve the same fluence at satellite orbit. We can account for such an altitude distribution by superposition of such results as derived above for sources at different altitudes. Assuming that the source strength distribution does not vary with altitude, this superposition simply involves summing the results derived as above for a variety of source altitudes, scaled by the number of TGFs at each altitude and with the maximum fluence shifted down by the additional attenuation in the atmosphere. Sources at different altitudes give similar spatial distributions of fluence, though sources at lower altitudes give slightly narrower distributions as shown for example for $\sigma_\theta = 30°$ in Figure 6a. The main difference then is in the fluence scale, as shown in Figure 6b.

[13] Compared to results for sources at a single high altitude, superposing results from sources at a variety of altitudes can only soften the observed fluence distribution. This is because sources at lower altitudes only contribute additional observations at fluences lower than that of a bright, high-altitude source detected from a nearby location. The degree of the softening depends on the nature of the altitude distribution. Sample observed fluence distributions for a variety of altitude distributions are shown in Figure 7 for a source with beam width $\sigma_\theta = 30°$ and strength distribution power law index $\alpha = 2$. While sources below 15 km altitude cannot explain the observed average photon energy spectrum [*Dwyer and Smith*, 2005; *Carlson et al.*, 2007], the actual range of production altitudes likely extends below 15 km so here we set the domain of the altitude distributions to 10 to 20 km to span typical thunderstorm and tropopause altitudes and the altitudes of TGF-associated electrical activity [*Stanley et al.*, 2006; *Shao et al.*, 2010; *Lu et al.*, 2010]. The largest degree of softening is seen with a Gaussian altitude distribution centered at 15 km with a standard deviation of 1 km. This is due to the rapid change both in the number of TGF sources and the peak observed fluence (Figure 6b) as altitude varies. Broader altitude distributions tend to produce observed fluence distributions more dominated by high-altitude sources as such sources are more likely to be detected. As before, the observed fluence distributions are less perturbed by altitude distributions in fluence ranges away from the peak fluence, i.e. at left in Figure 7. This can be understood as a result of the $\alpha_d > 1.5$ behavior of sources at a single altitude. Suppose, as above, that a population of TGF sources at 20 km altitude produce a peak observed fluence of F_d = 100. As shown above, the observed fluence distribution increases as fluence decreases with roughly power law behavior and $\alpha_d > 1.5$, implying that the 20 km altitude sources produce at least $10^{1.5} \sim 30$ times more observations at F_d = 10 than at F_d = 100. From Figure 6, the peak fluence for sources at 15 km is reduced by a factor of 10 relative to sources at 20 km. Therefore, unless

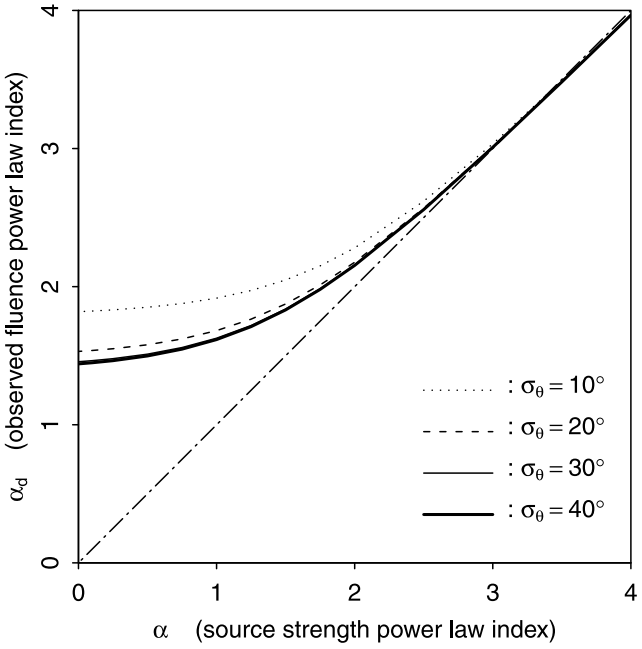

Figure 5. The power law index of the observed fluence vs the power law index of source strength for sources at 20 km altitude. The dotted, dashed, solid thin, and solid thick curves shown correspond to sources with σ_θ = 10°, 20°, 30°, and 40°, respectively, though the curves overlap for $\sigma_\theta \geq 30°$. The dash-dotted line shows $\alpha_d = \alpha$. For $\alpha \gtrsim 2.5$, $\alpha_d \simeq \alpha$, but for harder distributions of source strength the observed fluence distribution is significantly softened.

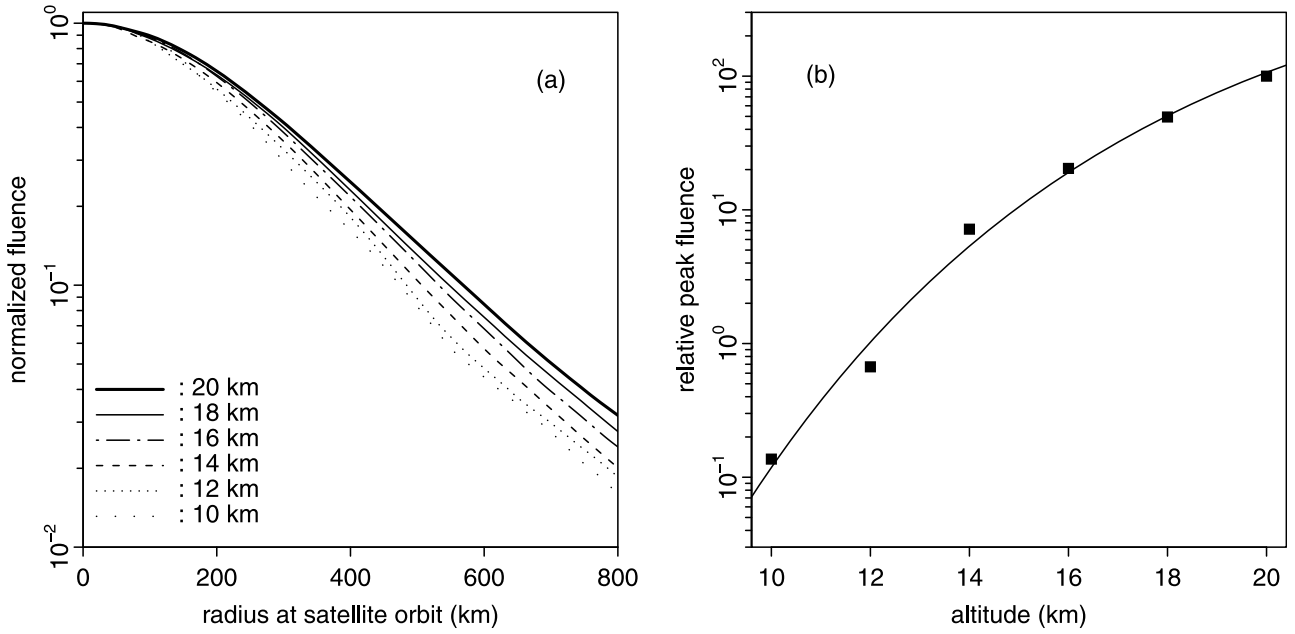

Figure 6. (a) A representative fluence distribution at satellite orbit shown for sources with $\sigma_\theta = 30°$ at a variety of altitudes, normalized to unity to compare distribution shapes. The curves represent, from bottom to top, 10, 12, 14, 16, 18, and 20 km source altitudes, as marked. (b) The peak fluence of a TGF of a given strength as a function of source altitude. The curve is a fit to the expected behavior for attenuation in an atmosphere with exponentially decreasing density.

there are at least 30× more sources at 15 km than at 20 km, the high-altitude sources will tend to dominate. The altitude distribution of TGF sources must rise rapidly as altitude decreases if the lower-altitude sources are to contribute a significant fraction of the observations. In the context of the observed fluence distribution, since the peak observed fluence tends to come from sources at the highest altitudes, the region of the fluence distribution away from the peak fluence tends to be dominated by the strength distribution of sources at the highest altitudes. In essence, the observed fluence distribution in regions away from the peak observed fluence tends to show the effects of the source strength distribution, not the altitude distribution.

6. Discussion

[14] The results in Figure 5 show the expected behavior of the fluence distribution of TGF measurements as a function of the distribution of source strength for sources at a single altitude. Figure 7 shows the effects of the source altitude distribution and suggests that the effects of the altitude distribution are relatively small for portions of the observed fluence distribution away from the peak observed fluence. Comparison with the observed distribution of TGF fluence in principle then allows us to determine the distribution of source strength. For instance, the distribution of TGF fluences observed by RHESSI [*Grefenstette et al.*, 2009, Figure 8] can be fit by power laws with index αd between 3 and 4, suggesting a source strength power law distribution with $\alpha \sim \alpha_d$. In practice, however, this comparison is complicated by issues with satellite measurement such as dead time and triggering efficiency. Dead time acts to soften the observed fluence distribution by reducing the fluence of high-fluence events

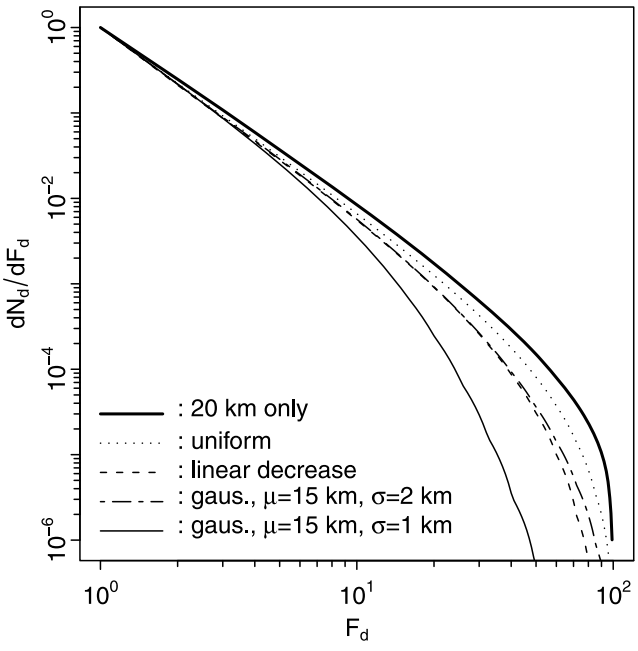

Figure 7. Sample observed fluence distributions for a variety of altitude distributions of a source with beam width $\sigma_\theta = 30°$ and power law source strength distribution with $\alpha = 2$. The thick solid curve is for sources at 20 km altitude, while the dotted, dashed, dash-dotted, and thin solid curves represent distributions between 10 and 20 km altitude that are respectively uniform, linearly decreasing, broad Gaussian (mean 15 km, standard deviation 2 km), and narrow Gaussian (mean 15 km, standard deviation 1 km) as indicated.

(especially relevant for RHESSI and earlier observations by the Burst And Transient Source Experiment, BATSE), while lower triggering efficiency for short, low-fluence events acts to harden the spectrum (especially relevant for BATSE and Fermi). One way to sidestep these difficulties is to compare the total rate of TGF detection of different satellites. Assuming differences in TGF detection rate are due to the different minimum detectable fluences for each satellite, one can construct a measure of the steepness of the fluence distribution. Alternatively, correcting the data for dead-time can provide a direct estimate of the fluence distribution. Preliminary analysis suggests $\alpha_d \sim 2.0$. Further results are forthcoming.

[15] The fluence distribution can, as in Figure 5, be used to determine the properties of the source strength distribution. The source strength distribution in turn has direct relevance to the source physics. A power law source strength distribution would not be unexpected as many dynamical systems, especially those displaying slow buildup until breakdown, evolve to a critical point with scale invariance and a power law spectrum of breakdown events [*Bak et al.*, 1987]. The exact source strength distribution power law index and the cutoffs of the distribution, if any, are characteristics of the physics of the source. These characteristics can therefore be used to constrain the physics responsible for TGF emission. There is some evidence for a minimum intensity cutoff provided by the ADELE observations [*Smith et al.*, 2011], though the nature of the threshold is unknown. Such a threshold, together with the power law index and a normalization from satellite observations, can be used to determine the global TGF frequency, a key unknown in determining the global importance of TGFs. Present estimates of global TGF frequency span a wide range, including a lower limit of 50/day on the basis of TGF observations [*Smith et al.*, 2005], an estimate of 1500/day on the basis of electron emissions in conjunction with TGFs [*Carlson et al.*, 2011], and an order of magnitude estimate of 15,000/day on the basis of the ADELE observations [*Smith et al.*, 2011]. We hope that the connections derived above between source strength and observed fluence can be used to refine these estimates. Further analysis of TGFs observed with the RHESSI, AGILE, and Fermi satellites and future observations with the upcoming TARANIS and ASIM instruments will provide better estimates of the observed fluence distribution, and further ground and aircraft observations close to lightning can be used to determine the nature of the distribution at low source strengths.

[16] **Acknowledgments.** This work was supported by Norwegian Research Council grant 197638/V30.

[17] Robert Lysak thanks the reviewers for their assistance in evaluating this paper.

References

Agostinelli, S., et al. (2003), GEANT4—A simulation toolkit, *Nucl. Instrum. Methods Phys. Res., Sect. A*, *506*(3), 250–303, doi:10.1016/S0168-9002(03)01368-8.

Bak, P., C. Tang, and K. Wiesenfeld (1987), Self-organized criticality: An explanation of the 1/f noise, *Phys. Rev. Lett.*, *59*(4), 381–384, doi:10.1103/PhysRevLett.59.381.

Briggs, M. S., et al. (2010), First results on terrestrial gamma ray flashes from the Fermi Gamma-ray Burst Monitor, *J. Geophys. Res.*, *115*, A07323, doi:10.1029/2009JA015242.

Carlson, B. E., N. G. Lehtinen, and U. S. Inan (2007), Constraints on terrestrial gamma ray flash production from satellite observation, *Geophys. Res. Lett.*, *34*, L08809, doi:10.1029/2006GL029229.

Carlson, B. E., N. G. Lehtinen, and U. S. Inan (2009), Terrestrial gamma ray flash production by lightning current pulses, *J. Geophys. Res.*, *114*, A00E08, doi:10.1029/2009JA014531.

Carlson, B. E., N. G. Lehtinen, and U. S. Inan (2010), Terrestrial gamma ray flash production by active lightning leader channels, *J. Geophys. Res.*, *115*, A10324, doi:10.1029/2010JA015647.

Carlson, B. E., T. Gjesteland, and N. Østgaard (2011), Terrestrial gamma-ray flash electron beam geometry, fluence, and detection frequency, *J. Geophys. Res.*, *116*, A11217, doi:10.1029/2011JA016812.

Celestin, S., and V. P. Pasko (2011), Energy and fluxes of thermal runaway electrons produced by exponential growth of streamers during the stepping of lightning leaders and in transient luminous events, *J. Geophys. Res.*, *116*, A03315, doi:10.1029/2010JA016260.

Chanrion, O., and T. Neubert (2010), Production of runaway electrons by negative streamer discharges, *J. Geophys. Res.*, *115*, A00E32, doi:10.1029/2009JA014774.

Cohen, M. B., U. S. Inan, and G. Fishman (2006), Terrestrial gamma ray flashes observed aboard the Compton Gamma Ray Observatory/Burst and Transient Source Experiment and ELF/VLF radio atmospherics, *J. Geophys. Res.*, *111*, D24109, doi:10.1029/2005JD006987.

Cohen, M. B., U. S. Inan, R. K. Said, and T. Gjestland (2010), Geolocation of terrestrial gamma-ray flash source lightning, *Geophys. Res. Lett.*, *37*, L02801, doi:10.1029/2009GL041753.

Connaughton, V., et al. (2010), Associations between Fermi Gamma-ray Burst Monitor terrestrial gamma ray flashes and sferics from the World Wide Lightning Location Network, *J. Geophys. Res.*, *115*, A12307, doi:10.1029/2010JA015681.

Cummer, S. A., Y. Zhai, W. Hu, D. M. Smith, L. I. Lopez, and M. A. Stanley (2005), Measurements and implications of the relationship between lightning and terrestrial gamma ray flashes, *Geophys. Res. Lett.*, *32*, L08811, doi:10.1029/2005GL022778.

Cummer, S. A., G. Lu, M. S. Briggs, V. Connaughton, S. Xiong, G. J. Fishman, and J. R. Dwyer (2011), The lightning-TGF relationship on microsecond timescales, *Geophys. Res. Lett.*, *38*, L14810, doi:10.1029/2011GL048099.

Dwyer, J. R. (2007), Relativistic breakdown in planetary atmospheres, *Phys. Plasmas*, *14*, 42901, doi:10.1063/1.2709652.

Dwyer, J. R. (2008), Source mechanisms of terrestrial gamma-ray flashes, *J. Geophys. Res.*, *113*, D10103, doi:10.1029/2007JD009248.

Dwyer, J. R., and D. M. Smith (2005), A comparison between Monte Carlo simulations of runaway breakdown and terrestrial gamma-ray flash observations, *Geophys. Res. Lett.*, *32*, L22804, doi:10.1029/2005GL023848.

Fishman, G. J., et al. (1994), Discovery of intense gamma-ray flashes of atmospheric origin, *Science*, *264*(5163), 1313–1316, doi:10.1126/science.264.5163.1313.

Gjesteland, T., N. Østgaard, P. H. Connell, J. Stadsnes, and G. J. Fishman (2010), Effects of dead time losses on terrestrial gamma ray flash measurements with the Burst and Transient Source Experiment, *J. Geophys. Res.*, *115*, A00E21, doi:10.1029/2009JA014578.

Gjesteland, T., N. Ostgaard, A. B. Collier, B. E. Carlson, M. B. Cohen, and N. G. Lehtinen (2011), Confining the angular distribution of terrestrial gamma-ray flash emission, *J. Geophys. Res.*, *116*, A11313, doi:10.1029/2011JA016716.

Grefenstette, B. W., D. M. Smith, B. J. Hazelton, and L. I. Lopez (2009), First RHESSI terrestrial gamma ray flash catalog, *J. Geophys. Res.*, *114*, A02314, doi:10.1029/2008JA013721.

Hazelton, B. J., B. W. Grefenstette, D. M. Smith, J. R. Dwyer, X.-M. Shao, S. A. Cummer, T. Chronis, E. H. Lay, and R. H. Holzworth (2009), Spectral dependence of terrestrial gamma-ray flashes on source distance, *Geophys. Res. Lett.*, *36*, L01108, doi:10.1029/2008GL035906.

Hedin, A. E. (1991), Extension of the MSIS thermosphere model into the middle and lower atmosphere, *J. Geophys. Res.*, *96*(A2), 1159–1172, doi:10.1029/90JA02125.

Inan, U. S., S. C. Reising, G. J. Fishman, and J. M. Horack (1996), On the association of terrestrial gamma-ray bursts with lightning and implications for sprites, *Geophys. Res. Lett.*, *23*(9), 1017–1020, doi:10.1029/96GL00746.

Inan, U. S., M. B. Cohen, R. K. Said, D. M. Smith, and L. I. Lopez (2006), Terrestrial gamma ray flashes and lightning discharges, *Geophys. Res. Lett.*, *33*, L18802, doi:10.1029/2006GL027085.

Lu, G., et al. (2010), Lightning mapping observation of a terrestrial gamma-ray flash, *Geophys. Res. Lett.*, *37*, L11806, doi:10.1029/2010GL043494.

Lu, G., S. A. Cummer, J. Li, F. Han, D. M. Smith, and B. W. Grefenstette (2011), Characteristics of broadband lightning emissions associated with terrestrial gamma ray flashes, *J. Geophys. Res.*, *116*, A03316, doi:10.1029/2010JA016141.

Marisaldi, M., et al. (2010), Detection of terrestrial gamma ray flashes up to 40 MeV by the AGILE satellite, *J. Geophys. Res.*, *115*, A00E13, doi:10.1029/2009JA014502.

Moss, G. D., V. P. Pasko, N. Liu, and G. Veronis (2006), Monte Carlo model for analysis of thermal runaway electrons in streamer tips in transient luminous events and streamer zones of lightning leaders, *J. Geophys. Res.*, *111*, A02307, doi:10.1029/2005JA011350.

Østgaard, N., T. Gjesteland, J. Stadsnes, P. H. Connell, and B. Carlson (2008), Production altitude and time delays of the terrestrial gamma flashes: Revisiting the Burst and Transient Source Experiment spectra, *J. Geophys. Res.*, *113*, A02307, doi:10.1029/2007JA012618.

Shao, X.-M., T. Hamlin, and D. M. Smith (2010), A closer examination of terrestrial gamma-ray flash-related lightning processes, *J. Geophys. Res.*, *115*, A00E30, doi:10.1029/2009JA014835.

Smith, D. M., L. I. Lopez, R. P. Lin, and C. P. Barrington-Leigh (2005), Terrestrial gamma-ray flashes observed up to 20 MeV, *Science*, *307*(5712), 1085–1088, doi:10.1126/science.1107466.

Smith, D. M., et al. (2011), The rarity of terrestrial gamma-ray flashes, *Geophys. Res. Lett.*, *38*, L08807, doi:10.1029/2011GL046875.

Stanley, M. A., X.-M. Shao, D. M. Smith, L. I. Lopez, M. B. Pongratz, J. D. Harlin, M. Stock, and A. Regan (2006), A link between terrestrial gamma-ray flashes and intracloud lightning discharges, *Geophys. Res. Lett.*, *33*, L06803, doi:10.1029/2005GL025537.

B. E. Carlson, T. Gjesteland, and N. Østgaard, Department of Physics and Technology, University of Bergen, Allégaten 55, N-5007 Bergen, Norway. (brant.carlson@ift.uib.no)